TRANSPORTES
revistatransportes.org.br
anpet
associação nacional de pesquisa e ensino em transportes
anpet.org.br

Effect of different types of fine aggregates on fatigue resistance and self-healing of fine aggregate asphalt matrices

Efeito de diferentes tipos de agregados finos na resistência a fadiga e na capacidade de cura de matriz asfáltica de agregado fino

Miguel Faé Linhares[1], Jamilla Emi Sudo Lutif Teixeira[2], Verônica Teixeira Franco Castelo Branco[3], Wellington Lorran Gaia Ferreira[4]

[1]Federal University of Espírito Santo, Vitória, Espirito Santo, Brasil
[2]University of Nebraska, Lincoln, Nebraska, United States
[3]Federal University of Ceará, Fortaleza, Ceará, Brasil
[4]Federal Rural University of the Semiarid, Caraúbas, Rio Grande do Norte, Brasil

Contact: miguelfae@gmail.com, (MFL); jamilla.teixeira@unl.edu, (JESLT); veronica@det.ufc.br, (VTFCB); wellington.ferreira@ufersa.edu.br, (WLGF)

Submitted:
9 March, 2024
Revised:
16 June, 2024
Accepted for publication:
17 June, 2024
Published:
19 August, 2024
Associate Editor:
Francisco Thiago Sacramento Aragão, Universidade Federal do Rio de Janeiro, Brasil

Keywords:
Fine aggregate matrix.
Aggregate mineralogy.
Fatigue.
Self-healing.

Palavras-chave:
Matriz de agregado fino.
Mineralogia do agregado.
Fadiga.
Autocura.

DOI: 10.58922/transportes.v32i2.2997

OPEN ACCESS
CC BY

ABSTRACT
Fatigue cracking is one of the most common types of distress in asphalt pavements. Each asphalt concrete (AC) constituent and its interactions are relevant to characterize the resistance to fatigue cracking of the ACs. Also, for the selection of materials, it is essential to consider not only the capacity of the material resist to fatigue cracking but also its ability to heal. Materials owning self-heal properties can enlarge the ACs fatigue life. Many former studies investigated the self-healing of bituminous materials at the binder level. However, this material property can be dependent on the binder-aggregate interactions. Thus, the current work aims to evaluate the influence of using different fine aggregates on the fatigue cracking resistance and self-healing capacity behavior of fine aggregate matrices (FAMs). First, granite, basalt, and mica schist aggregates were subjected to physical, morphological, and mineralogical characterization. Then, three FAMs were fabricated with the same asphalt binder and these different fine aggregates. To evaluate the fatigue cracking resistance and self-healing capacity of the FAMs, frequency sweep and time sweep tests were conducted. The simplified viscoelastic continuum damage (S-VECD) theory was used to interpret the results of those tests. The mineral composition of the aggregates impacted the stiffness and the fatigue life of the FAMs. However, there was no significant influence of the aggregates on the self-healing capacity of the FAMs, since there was no significant increase in the fatigue life of the materials after the resting periods in the time sweep tests.

RESUMO
O trincamento por fadiga é um dos tipos de desgaste mais comuns em pavimentos asfálticos. Cada constituinte do Concreto Asfáltico (CA) e suas interações são relevantes para caracterizar a resistência ao trincamento por fadiga dos CAs. Além disso, para a seleção dos materiais, é essencial considerar não apenas a capacidade do material de resistir ao trincamento por fadiga, mas também a sua capacidade de cura. Materiais que possuem propriedades de autocura podem aumentar a vida de fadiga. Muitos estudos investigaram a autocura de materiais betuminosos ao nível do ligante asfáltico. No entanto, esta propriedade do material pode depender das interações ligante-agregado. Assim, o presente trabalho tem como objetivo avaliar a influência da utilização de diferentes agregados finos na resistência ao trincamento por fadiga e na capacidade de autocura de Matrizes de Agregados Finos (MAFs). Primeiramente, agregados do tipo granito, basalto e micaxisto foram submetidos à caracterização física, morfológica e mineralógica. Em seguida, foram fabricadas MAFs com o mesmo ligante asfáltico utilizando os três diferentes agregados finos. Para avaliar a

resistência ao trincamento por fadiga e a capacidade de autocura das MAFs, foram realizados testes de varredura de frequência e varredura de tempo. A teoria simplificada do dano contínuo viscoelástico (S-VECD) foi utilizada para interpretar os resultados desses testes. A composição mineral dos agregados impactou a rigidez e a vida de fadiga das MAFs. Porém, não houve influência significativa dos agregados na capacidade de autocura, uma vez que não houve aumento significativo na vida de fadiga dos materiais após os períodos de repouso nos ensaios de varredura de tempo.

1. INTRODUCTION

Fatigue cracking in asphalt concrete (AC) is one of the most common types of distress in flexible pavements, and it is a result of the cumulative surface damage due to the repetitive traffic loading leading to microcracking initiation, evolution, and coalescence to macrocracks. However, as mentioned by many authors (Daniel and Kim, 2001; Kim, Little and Lytton, 2003; Palvadi et al., 2012; Pivetta, Nascimento and Brito, 2020), when asphalt materials are micro-cracked, in response they are also able to heal when not loaded. Self-healing is a complex physical and chemical process that gradually closes the cracks, recovering partially the original properties of the material (Palvadi, Bhasin and Little, 2012).

For asphalt materials, self-healing is usually quantified by the partial recovery of the material stiffness after a damaged sample is allowed to rest. The partial stiffness recovery is a complex phenomenon and can be attributed to reversible effects, such as thixotropy, self-heating, and nonlinear effects, and/or because of irreversible phenomena such as damage due to microcrack initiation and growth (Oliveira, Babadopulos and Soares, 2021). As self-healing characteristic is inherited from the asphalt binder, most of the studies are focused on the binder phase. However, the AC is a complex composite where any microstructure response is ruled not only by the binder itself, but also by its constituents (binder, aggregates, and air voids) and how they are distributed and interact within the mixture.

In this context, a poor binder-aggregate adhesion can lead to cracks, and this is also dependent on the aggregate type (Moreno and Rubio, 2013; Xu and Wang, 2016; Moura et al., 2020). Even though different aggregates have similar physical characteristic (such as gradation), the morphological, and the mineralogical properties might be different, and it may impact the fatigue resistance of the AC (Masad et al., 2005; Zhang et al., 2015; Cala et al., 2019). In addition, concerning the self-healing, Li et al. (2023) found that the presence of taconite waste (a material that has metallic oxide as its main component) increased the healing capacity of the asphalt binder, mainly because the presence of metallic components increased the thermal conductivity of the binder. Phan, Park and Le (2018) and Li, Karki and Hao (2020) evaluated the impact of steel slag as an aggregate in AC for self-healing purposes and found an improvement in self-healing when infrared heating is applied to heal, as the metallic components increase thermal conductivity as well.

To evaluate the fatigue behavior of the AC, the intermediate length-scale called fine aggregate matrix (FAM) has been used by some authors (Freire, Castelo Branco and Vasconcelos, 2014; Klug, Ng and Faxina, 2022). The FAM constituents are asphalt binder, air voids, filler, and fine aggregates. Since coarse aggregate particles with varied particle size distribution and orientation are not included in the FAM, a more uniform internal structure is obtained, thus reducing the variability of the results of experimental tests. Many research efforts already showed correlation between FAM fatigue resistance and AC performance (Kim, Little and Song, 2003; Freire, Castelo Branco and Vasconcelos, 2014; Freire et al., 2017). Previous studies also show the effect of binder type and content (Shen, Chiu and Huang, 2010), aggregate particle size (Freire et al., 2017), and different fillers (Kim, Little and Song, 2003) on the FAM performance.

Palvadi, Bhasin and Little (2012) proposed a methodology to quantify FAM fatigue resistance and self-healing characteristics based on the simplified viscoelastic continuum damage (S-VECD) model, using mixtures with a single aggregate source but different binders. Karki et al. (2015) proposed a method to quantify both damage and self-healing characteristics of FAM coupling different rest periods in the same test routine. Li, Karki and Hao (2020) applied the method proposed by Karki et al. (2015) to assess the fatigue cracking resistance and self-healing of FAM composed of natural asphalt (rock asphalt). However, in these studies limited information was provided on fine aggregates and, as previously mentioned, the aggregate characteristic can also influence the behavior of the material, especially at the microstructure level, where microcracking and self-healing are most impactful.

In this context, this research is concerned to investigate the impact of different fine aggregates on fatigue resistance and self-healing capacity. The first goal is characterizing three different aggregates (granite, basalt, and mica schist) considering physical, morphological, and mineralogical properties. Secondly, frequency sweep tests, within the linear-viscoelastic region, and time sweep tests, with resting periods, were conducted on FAM samples to assess the healing capacity considering the S-VECD model. This approach is guided by the fact that some intrinsic characteristics of the fine aggregates may help to better understand the healing phenomenon since the blending between asphalt binder and fine aggregates creates an important portion of the AC which may govern the microstructure response of the material, including the microcracking initiation, propagation, and healing.

2. MATERIALS AND METHODS

2.1. Materials

2.1.1. Aggregate characterization

Three types of aggregates commonly found in Brazil were selected in order to study a variety of aggregates sources: i) granite aggregate (GRJ), collected from the state of Rio de Janeiro/BR; ii) basaltic aggregate (BA), originated from mafic rocks, collected from the state of Espírito Santo/BR; and iii) mica schist aggregates (MX), originated from metamorphic rocks, collected from the state of Goiás/BR. Each aggregate was sieved through sieve No. 10 (#2.0 mm), which was the nominal maximum aggregate size (NMAS) selected for the FAM, based on Freire et al. (2017). After sieving, the material was homogenized, and oven dried at 105 °C.

The physical characterization included the specific gravity and water absorption of the particles with size distribution between 2.00 mm and 0.075 mm, by DNIT 411/2019 specifications (DNIT, 2019). Specific gravity of particles smaller than 0.075mm was determined according to ABNT NBR 16605:2017 (ABNT, 2017). The gradation analysis was conducted specifically for particles smaller than 0.063mm, as the filler component significantly impacts the stiffening and healing properties of asphalt binders (Mazzoni, Stimilli and Canestrari, 2016). For that, a laser diffraction equipment (Mastersizer 2000 - Malvern Instruments) was employed.

In order to obtain aggregate shape properties, the aggregate image measurement system (AIMS) was used following the methods and classification proposed by Ibiapina et al. (2018) for Brazilian aggregates. The angularity of each particle was determined by analyzing the angles of the edges in the 2D images, with the parameter value ranging from 0 to 10,000. A higher value indicates a more angular particle, while a value closer to 0 represents a more rounded particle. The 2D shape

parameter was used to evaluate the shape of the aggregates, differentiating between elongated and circular particles. This parameter ranges from 0 to 20, where 0 represents a perfect circle, and 20 indicates a more elongated particle.

In addition to the analysis performed in AIMS, a scanning electron microscope (SEM) was employed. The SEM allowed imaging the particles, providing valuable insights into their shape, texture, and surface features. Besides, with the SEM and the energy dispersive spectroscopy (EDS) it was possible to identify the chemical elements presented on the aggregates size between 0.425 mm and 0.150 mm.

Lastly, it was essential to identify the main minerals present in each aggregate. The mineralogical compositions were determined using X-ray diffraction (XRD) analysis conducted on an Ultima IV - Rigaku diffractometer equipped with a molybdenum anode tube. The diffractogram data were analyzed using the Match! software, which employs the Crystallography Open Database (COD, 2021) for mineral identification and analysis. The physical, morphological, and mineralogical characterization was performed considering the particle size, as illustrated in Figure 1.

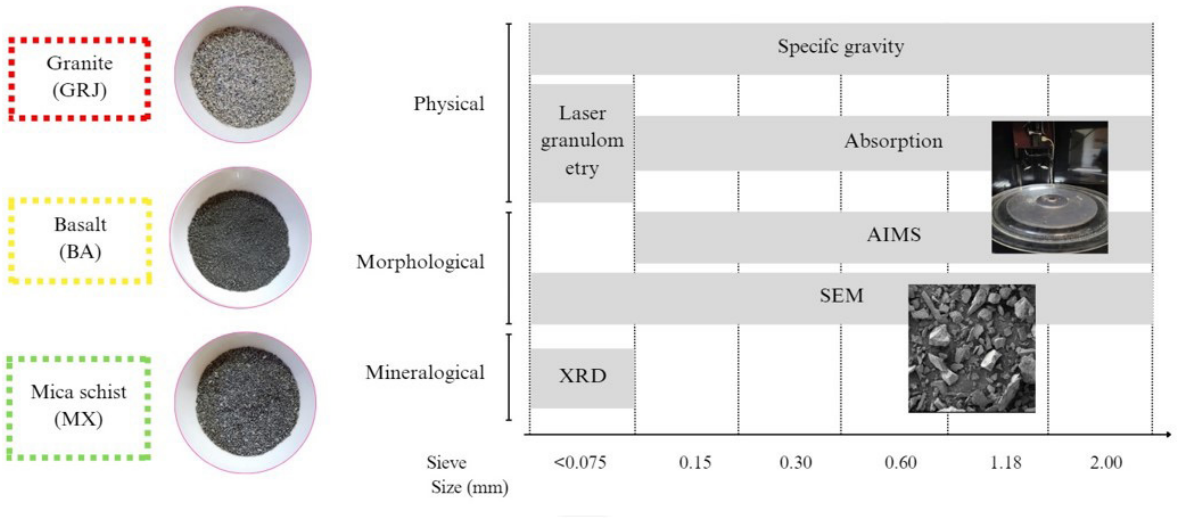


Figure 1. Aggregate types and characterization based on the particle size.

2.1.2. FAM mix design and compaction procedure

Three FAMs were so-called according to the aggregate type, i.e., FAM_GRJ, FAM_BA, and FAM_MX, corresponding to granite, basaltic, and mica schist aggregates, respectively. The overall particle size distribution (PSD) was maintained as the same to avoid the effect of the gradation on the results. The PSD was defined based on a typical AC gradation curve included in lower and upper limits of Brazilian DOT limits (DNIT_C range) usually adopted to produce dense-graded asphalt mixtures for surface course applications (DNIT, 2006).

To produce the FAM, an unmodified binder with a penetration grade - PEN 30/45 from Refinaria Duque de Caxias – REDUC (located in Rio de Janeiro, BR) was selected, with softening point of 52 °C, specific gravity of 1.054, and Brookfield viscosity of 508 Cp, 246 Cp, and 88 Cp at 135 °C, 150 °C, and 177 °C, respectively. The FAM_GRJ binder content was determined following the FAM mix design method proposed by Ng et al. (2018). A target air void content of 4.0 ± 0.5% was

established for all samples. Then, for the other FAMs, since the binder film thickness also influences the FAM resistance to fatigue cracking and self-healing (Abo-Qudais and Suleiman 2005; Ayar, Moreno-Navarro and Rubio-Gámez, 2016), the binder content (in volume) of each FAM was kept as close as possible to minimize the effects of this variable in the analysis. Table 1 presents the gradation and the binder content of each FAM.

Table 1 - Gradation and binder content of each FAM.

FAM ID	Binder (%)	Aggregate (%)			
		2.00-0.425mm	0.425-0.150mm	0.150-0.075mm	< 0.075mm
FAM_GRJ	10.3	40.7	22.1	21.5	5.5
FAM_BA	9.7	40.9	22.2	21.7	5.5
FAM_MX	10.3	40.6	22.0	21.5	5.7

FAM samples can be obtained either by extraction from large Superpave Gyratory Compactor (SGC) samples or produced individually using a procedure first developed by Kim et al. (2003) and adopted by other researchers (Fonseca et al., 2019; Rodrigues et al., 2019). In this study, cylindrical FAM samples with 12 mm in diameter and 50 mm in height were fabricated individually and following the procedure adopted by many other researchers (Kim, Little and Lytton, 2003; Castelo Branco et al., 2008; Vasconcelos, Bhasin and Little, 2010; Freire et al., 2017). Figure 2 illustrates the compaction protocol used herein.

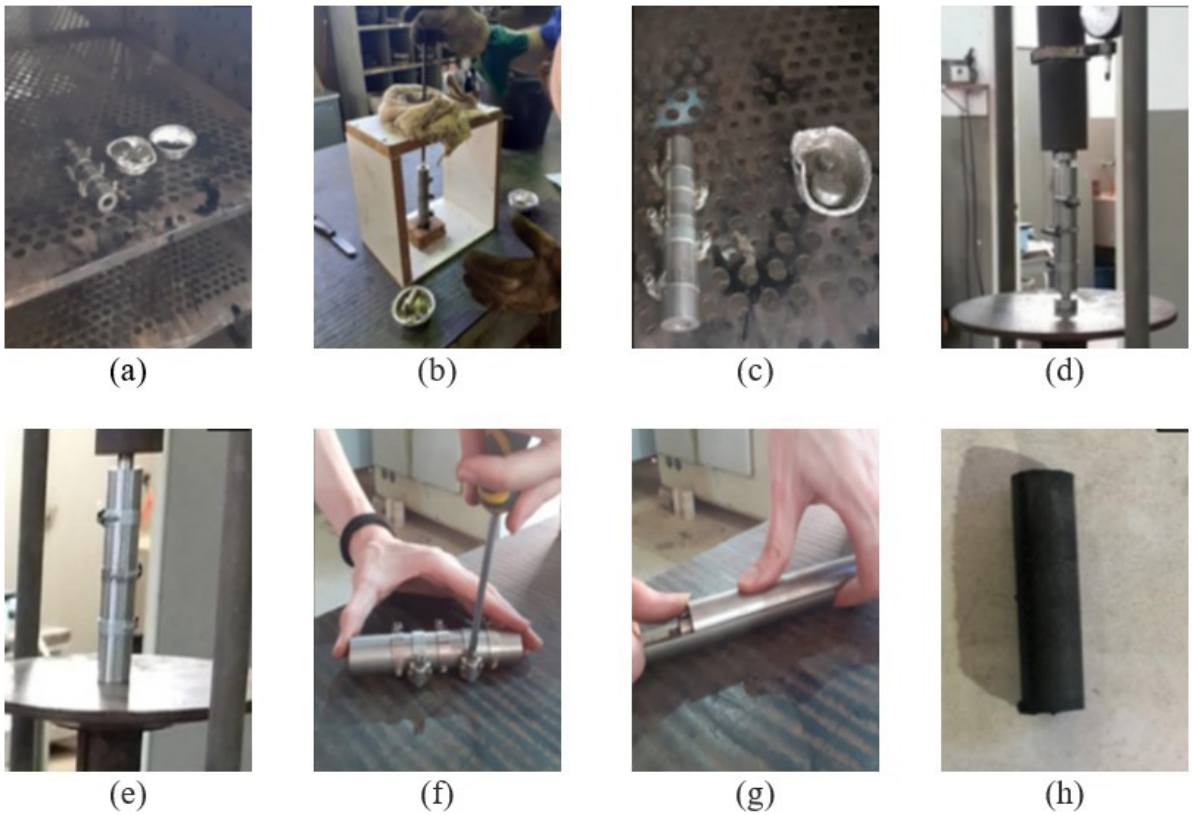


Figure 2. Compaction protocol for the FAM: (a) mold and mixture in the oven at 135 °C; (b) mixture poured into the mold; (c) mold with the mixture in the oven; (d) mold and CBR loading press; (e) detachment of the sample inside the mold; (f) opening of the screws that close the mold; (g) unmold; (h) final specimen.

First, the mold and the mixture were placed in an oven at 135 °C for 30 minutes (Figure 2a). Next, the prepared mixture was poured into the mold (Figure 2b). The mold, now filled with the FAM, was securely locked using clamps and returned to the oven for an additional 15 minutes (Figure 2c). Subsequently, the compacting process was conducted using a California Bearing Ratio (CBR) loading press (Figure 2d). The load was applied until there was no visible gap between the mold cover and the mold body. Once the compaction was complete, the sample is detached from the walls of the mold with the aid of the CBR loading pressure (Figure 2e). Finally, the compacted FAM was removed from the mold by disassembling the two halves of the mold (Figure 2f and 2g), and a cylindrical FAM sample was obtained (Figure 2h).

2.2. FAM fatigue and self-healing assessment

2.2.1. S-VECD model

The fatigue was assessed by measuring the number of cycles to failure (N_f) during the time sweep test, and the self-healing capacity of the FAMs were assessed by comparing parameters extracted from damage characteristic curves at different times (before and after resting period).

For that, the material integrity (C) and damage (S) parameters were obtained using the S-VECD modeling approach. The S-VECD model (developed by Daniel and Kim, 2002; and later adapted by Underwood, Baek and Kim, 2012) is a simplification of the continuous damage mechanics theory to account for the progressive damage in viscoelastic material. The pseudo-rigidity, C, is obtained for each loading cycle, and it is expressed by the relationship between the stress between peaks for each cycle (τ_{pp}) and the pseudo-strain of the material in that cycle, (γ_{pp}^{R}). This relationship is presented by Equation 1.

$$C(S) = \frac{\tau_{pp}}{\gamma_{pp}^{R} \times DMR} \tag{1}$$

where DMR is the dynamic modulus ratio, a correction factor that aims to reduce the variations from sample to sample. This factor is obtained by the ratio of the dynamic modulus obtained in the fatigue test ($\left|G^*\right|_{Initial}$) by the dynamic modulus obtained in the "fingerprint" test ($\left|G^*\right|_{Fingerprint}$), non-damage test, as shown in Equation 2.

$$DMR = \frac{\left|G^*\right|_{Initial}}{\left|G^*\right|_{Fingerprint}} \tag{2}$$

In turn, the pseudo-strain (γ^R) deals with the relationship between the linear viscoelastic stress of a given cycle (τ^R), by the reference modulus (G_R). As the dynamic modulus is given by Equation 3, the pseudo strain between peaks can be calculated through Equation 4.

$$\left|G^*\right| = \frac{\tau^R}{\gamma^R} \tag{3}$$

$$\gamma_{pp}^{R} = \frac{1}{G_R}\left(\gamma_{pp} \times \left|G^*\right|_{fingerprint}\right) \tag{4}$$

The calculation of the accumulated damage variable (S) until a given cycle is given by the sum of the damage generated in each load cycle (i) as presented in Equation 5. Where, the cycle start time (t_i), the end time (t_{i-1}) and the alpha exponent or rate of damage evolution (α) that can be obtained by Equation 6, through the slope of the master curve of the relaxation module of the material in log-log space (m_α).

$$S = \sum_{i=1}^{N} \left[\frac{DMR}{2} \left(\gamma_{pp}^{R} \right)^2 \left(C_{1-i}^{*} - C_{i}^{*} \right) \right]^{\frac{\infty}{1+\infty}} \times \left[t_i - t_{i-1} \right]^{\frac{1}{1+\infty}} \quad (5)$$

$$\alpha = \frac{1}{m_\alpha} \quad (6)$$

2.2.2. Oscillatory tests

The rheological tests were conducted using a dynamic shear rheometer (DSR) model DHR2 from TA Instruments. Firstly, frequency sweep tests, also known as fingerprint tests, were conducted at various frequencies (ranging from 25 Hz to 0.01 Hz), at 25 °C. A low torsional sinusoidal strain of 65 με was applied during these tests to ensure that the material was evaluated within its linear viscoelastic region (Freire et al., 2017; Sánchez et al., 2017).

Then, time sweep tests at 25 °C and a frequency of 10 Hz were conducted to perform the fatigue life characterization on the FAM samples. Based on preliminary results, a stress-controlled loading level of 400 kPa was chosen to induce progressive fatigue damage in the specimen. The self-healing capacity was assessed by inducing a resting period of 60 min. during the time sweep test. The initiation of the resting period was applied when the sample lost 20% of its initial dynamic modulus, i.e., the pseudo-stiffness value dropped to an integrity of 80% (C_{80}). Thus, the fatigue life (N_f) criterion adopted was based on the phase angle abrupt drop.

The damage characteristic curve (C × S) can be obtained from a curve before the resting time, adding a shifted time sweep curve obtained after a resting period (Figure 3a). To this end, the parcel of the curve related to self-healing and/or other reversible effects must be eliminated. More details can be found elsewhere (Karki et al., 2015). Figure 3b illustrates the final C × S curve.

In order to quantify the self-healing characteristics of the FAMs, the increment in the pseudo-stiffness value was adjusted to a corresponding increment in stiffness, denoted as *C'f*, relative to its initial C × S curve, without resting period. This approach, introduced by Karki et al. (2015), accounts for the apparent disparity between *Cf* and *C'f*, which arises from a disproportionate increase in material stiffness, resulted from other reversible effects. Thus, the self-healing index (%H) is quantified using the relationship between the damage variable S_i, obtained at t_i, defined as the time when the fatigue test was interrupted, and S'_f, obtained at t_f, defined as the time when the fatigue test retakes, as described in Equation 7.

$$\%H = \frac{S_i - S'_f}{S_i} \times 100 \quad (7)$$

Furthermore, to verify if the changes in material integrity (pseudo-stiffness) could be attributed to the self-healing phenomena, the increase in the FAM fatigue life was calculated, including resting periods, and compared to its correspondent curve without resting periods. It is expected that if a noticeable self-healing happens, a meaningful change in the material fatigue life should appear.

Samples from fingerprint tests were used for the time sweep tests after a resting period of 30min., to ensure the recovery of reversible effects caused during fingerprint tests. After that, time sweep tests were initiated. The resting period of 60min. was applied after finding that pseudo stiffness reduced to 80% of its initial value. Then, the tests were conducted up to the complete failure.

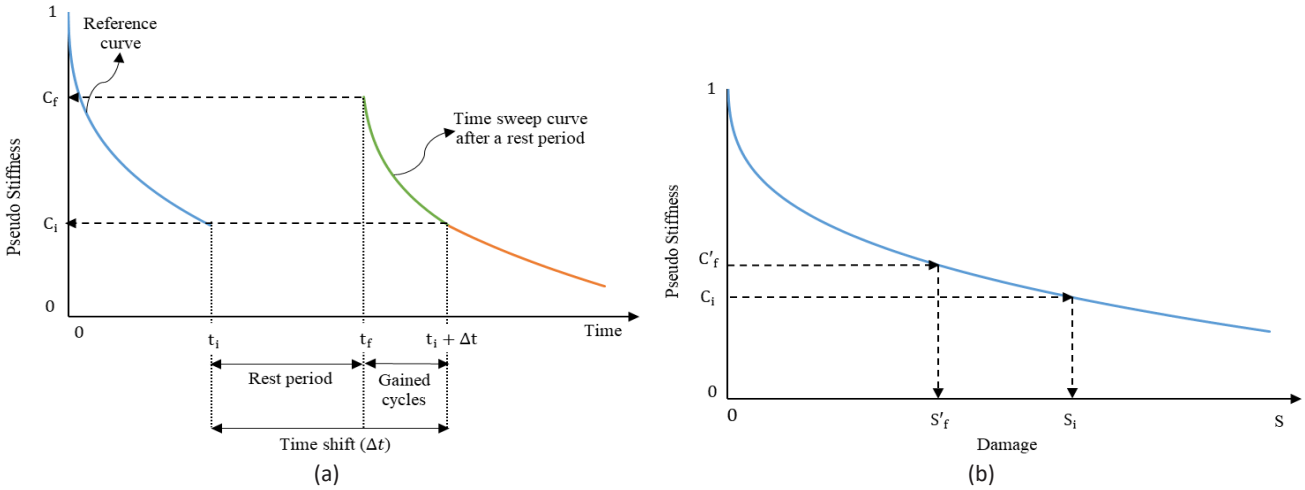


Figure 3. (a) Shifting the time sweep curve for calculating self-healing (Karki et al., 2015), and (b) C × S curve after shifting.

3. RESULTS AND DISCUSSIONS

3.1. Aggregates

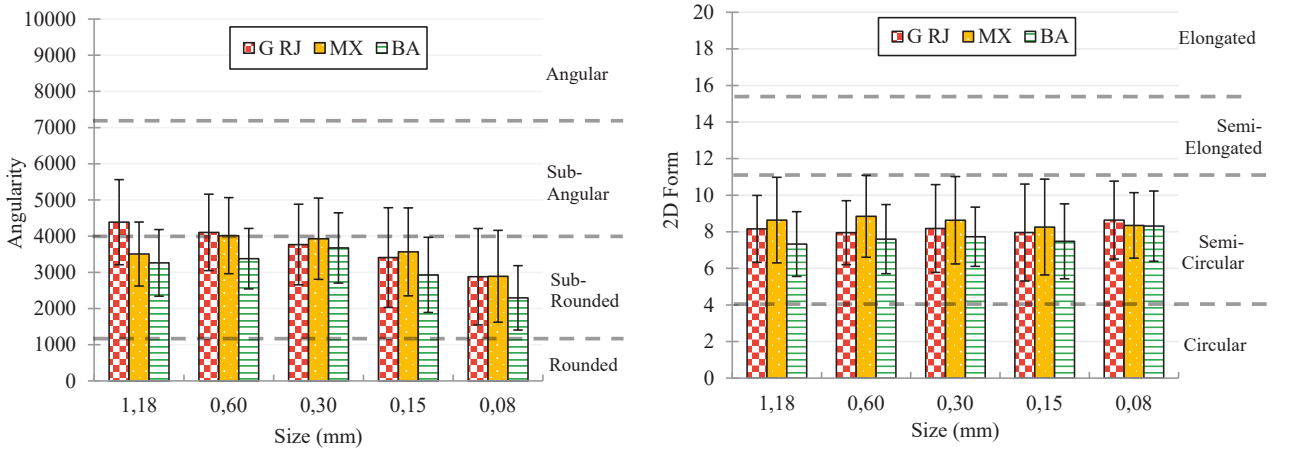
Table 2 presents the results of the specific gravity, absorption, and laser granulometry. Regarding absorption (2.00 mm to 0.075 mm particle sizes), BA had the highest absorption value (1.22%) among the three materials, while the MX had the smallest (0.28%). While the filler fraction of the aggregates GRJ and MX have a similar grain size distribution, the basalt filler presented a higher content of fines (58% passing through size 0.020 mm).

Figures 4a and 4b present the shape properties results. In terms of classification, the three aggregates present sub-rounded angularity (except GRJ #1.18 mm) and semi-circular form, based on the classification proposed by Ibiapina et al. (2018) using aggregates from Brazil. Although differences were observed in the angularity value, with a slight decrease for smaller fractions, this trend is not significant to change the classification of the aggregates. Among the aggregates, BA presents less angularity and 2D form in all fractions, while MX has higher 2D form. In addition, as for the SEM imagens (Figure 4c), BA aggregate has a rougher texture, which might lead to better binder-aggregate physical adhesion.

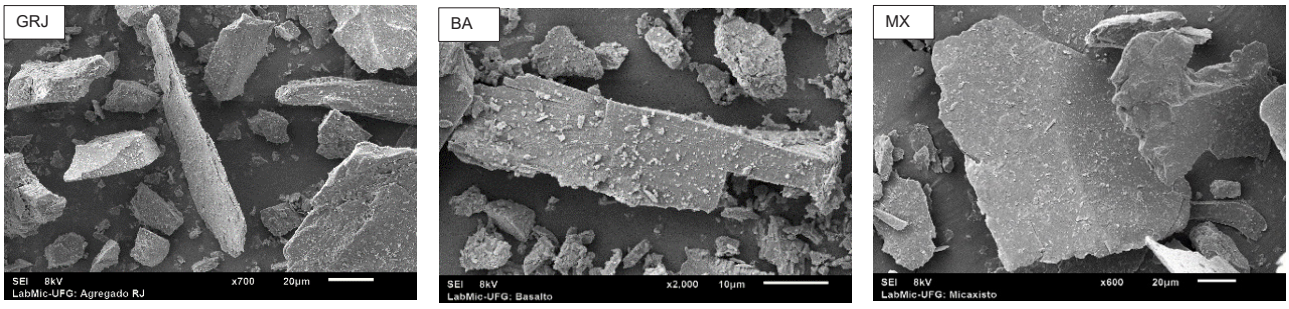
The percentage of each mineral, as well as the percentage of each chemical element are presented in Table 3. GRJ and MX present minerals such as quartz, feldspars (such as albite), and micas (such as muscovite and biotite) while BA particles present feldspars (such as labradorite), and pyroxenes (such as augite) minerals. In terms of chemical elements, it is highlighted the percentage of metal components (such as iron and aluminum) for the BA aggregates, which is reported as a self-healing improver (Phan, Park and Le, 2018; Li et al., 2020). On the other hand, SiO_2 (silicon dioxide) is known as a bad component to binder-aggregate adhesion, resulting in premature failure (Zhang et al., 2015; Cala et al., 2019).

Table 2 - Results of specific gravity, absorption, and laser granulometry.

Aggregate	Size (mm)		Specific Gravity	Absorption (%)	Passing (%)
GRJ	2.00-0.075		2.641	0.72	
	<0.075		2.680		
		0.001			2.0
		0.010			20.0
		0.020			38.0
BA	2.00-0.075		2.811	1.22	
	<0.075		2.838		
		0.001			3.0
		0.010			38.0
		0.020			58.0
MX	2.00-0.075		2.631	0.28	
	<0.075		2.782		
		0.001			1.0
		0.010			15.0
		0.020			32.0



(a) (b)



(c)

Figure 4. AIMS results (a) angularity and (b) 2D form, and SEM imagens (c).

Table 3 - Percentages of the minerals and chemical elements.

(%)				(%)			
Mineral	**G RJ**	**BA**	**MX**	**Chemical Elements**	**G RJ**	**BA**	**MX**
Quartz	37.2	5.5	29.4	Silicon	67.9	52.8	57.2
Albite	44.9	-	28.8	Iron	6.4	15	11.5
Labradorite	-	47.6	-	Aluminum	12.9	14.9	18.3
Biotite	3.5	-	15.7	Calcium	2.6	7.2	0.9
Muscovite	10.1	-	19.6	Potassium	4.4	1.6	4.7
Augite	-	25.9	-	Magnesium	1.8	3.3	4.5
Magnetite	-	16.3	-	Sodium	2.8	3.3	1.8
Hornblende	4.2	-	-	Phosphor	-	0.8	-
Clinochlor	-	-	6.5	Titanium	1.3	0.9	1.0
Kaolinite	-	4.6	-				

Quartz is a hard and rigid mineral, which suggests that its presence in the asphalt mixture can lead to higher stiffness. In contrast, albite is a low-strength and low-stiffness mineral. GRJ aggregates present high presence of quartz (37.2%) and albite (44.9%) which may hide any influence of the quartz mineral on the asphalt material stiffness. On the other hand, labradorite and augite are durable and hard minerals, but still lower when compared to quartz. BA aggregates present the lowest percentage of quartz among all, 5.5%, which may impact material stiffness. Lastly, MX aggregates have a more uniform distribution of minerals, 29.4% of quartz, 28.8% of albite, and 35.3% of micas (such as biotite and muscovite, which are soft minerals). Besides, the muscovite ability to provide good adhesion between aggregate and asphalt binder, and the high percentage of quartz may contribute to the overall stiffness of the FAM produced with MX aggregates.

3.2. FAM linear - viscoelastic properties

The average dynamic shear modulus curve obtained for each FAM is shown in Figure 5, as well as the $|G^*|_{Fingerprint}$ and the alpha exponent (Equation 6). Four samples of FAM for each aggregate type were evaluated.

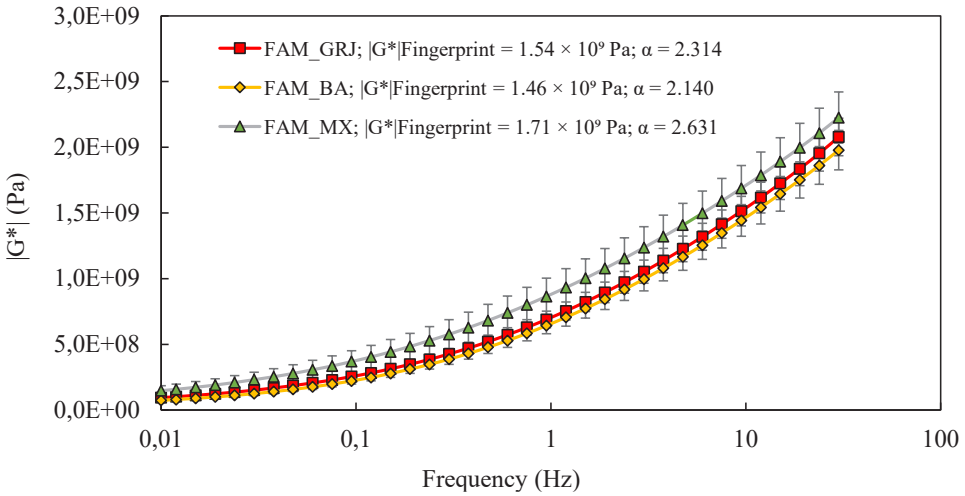


Figure 5. Dynamic shear modulus curve for each FAM.

It can be observed that the FAM_MX presented slightly higher values (around 1.3 times) of |G*| than the other FAMs. Considering that the FAMs were produced keeping the same aggregate particle distribution, binder content (in volume) as close as possible, all samples within the same air void range, and there was not found much difference in the shape properties of the aggregates by means of the AIMS, the differences found in the dynamic shear modulus might be related to aggregate mineralogical composition. MX is predominantly composed of quartz (29.4%), a mineral that contributes to stiffness gain. In contrast, FAM_BA presents a small quantity of quartz (5.5%).

3.3. FAM fatigue life and self-healing characteristics

Figure 6 shows the C × S curve, as well as the fitting parameters C_{11} and C_{12} from the power law function for each FAM. It can be observed that damage evolution rate is faster for FAM_MX when compared to the others. This can be attributed to the highest stiffness value found for FAM_MX. On the other hand, FAM_BA curve dropped faster as the damage increases, which also can be attributed to the lower stiffness of this FAM. C × S curves present important information related to internal microstructure changes due to cyclic loads, but it cannot be used directly to compare fatigue cracking resistance (Karki et al., 2015), because the fatigue resistance is dependent of two mechanisms, the ability of the material to dissipate energy through deformation and the energy dissipation due to cracking.

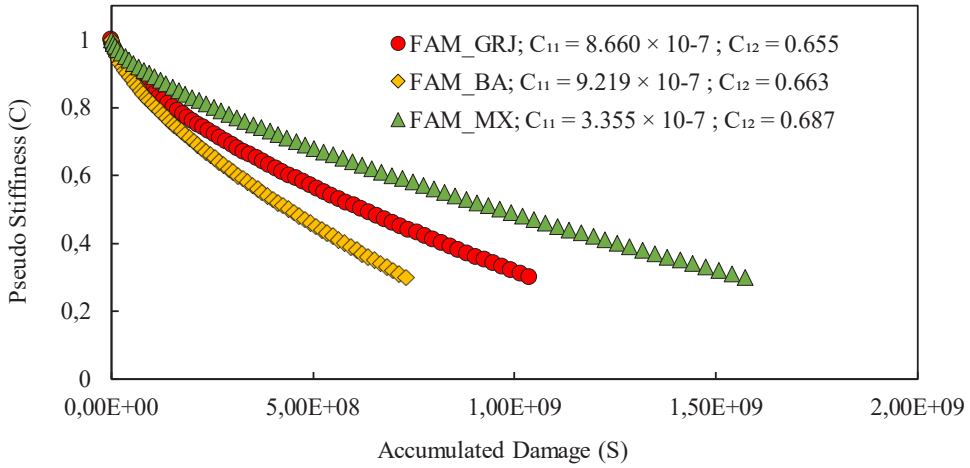


Figure 6. Damage characteristic curves of the FAMs.

Then, an analysis of the number of cycles to failure (N_f) and the healing percentual (%H) was conducted. Using the C × S results before and after the resting period (RP), the %H was calculated. Also, fatigue resistance with RP (w/RP) and without RP (w/no RP) were obtained. Thus, the increase in the fatigue resistance due to the RP was calculated. Table 4 shows the results for each FAM material, as well as the average values.

Table 4 shows that the percentage increase in fatigue life (average % N_f increase) was around the same magnitude for the three types of FAMs, about 8%. So, no significant difference was observed among the three aggregates. The great effects on the stiffness, and consequently on the material integrity, during rest is most likely related to reversible phenomena that do not directly influence the fatigue life. The same conclusion was stated by Babadopulos et al. (2019) and Oliveira, Babadopulos and Soares (2021).

Table 4 - Self-healing and fatigue life of each sample and average.

FAM Sample	H%	Average H%	N_f (w/ RP)	N_f (w/no RP)	$\%N_f$ Increase	Average $\%N_f$ increase
FAM_GRJ 01	17.35	18.41	1,664	1,540	8.1	8.3
FAM_GRJ 02	19.58		1,959	1,808	8.4	
FAM_GRJ 03	21.43		1,622	1,508	7.6	
FAM_GRJ 04	17.18		1,644	1,538	6.9	
FAM_GRJ 05	16.51		1,303	1,176	10.8	
FAM_BA 01	22.03	24.16	925	857	7.9	8.4
FAM_BA 02	22.39		587	553	6.1	
FAM_BA 03	31.88		876	801	9.4	
FAM_BA 04	20.32		1,004	911	10.2	
FAM_MX 01	13.07	14.10	1,992	1,809	10.1	8.0
FAM_MX 02	14.12		942	881	6.9	
FAM_MX 03	15.83		2,724	2,498	9.0	
FAM_MX 04	13.39		4,844	4,573	5.9	

It is important to highlight that the higher stiffness observed in FAM_MX could be the reason for the increase in the number of cycles to failure. But still, the results obtained showed that the load-related fatigue life is dependent on aggregate's characteristics. BA aggregates showed the highest absorption (1.22%, Table 2), which could also decrease the binder film thickness to dissipate energy through plastic deformation. In contrast, the MX aggregate has the lowest absorption (0.28%, Table 2), leading to a higher availability of binder increasing the binder film thickness.

4. CONCLUSIONS

This paper aimed to assess the influence of fine aggregate properties on FAM fatigue and self-healing capacity. Three types of fine aggregates were studied, and their physical, morphological, and mineralogical properties were evaluated. Subsequently, the rheological behavior of the FAMs was analyzed. The following conclusions were drawn:

- FAM_MX had better fatigue resistance than FAM_RJ and FAM_BA. This result was attributed to the greater stiffness observed in FAM_MX, due to the high presence of hard minerals such as quartz (29.40%), as well as the lower absorption (0.28%) which suggests a greater binder film thickness to dissipate energy. FAM_MX presented slightly higher values (around 1.3 times) of |G*| than the other FAMs. Materials with high stiffness experience low strain levels, leading to enhanced resistance against fatigue cracking. On the other hand, FAM_BA presented the lowest number of cycles to failure. This result could be attributed to the higher absorption (1.22%) of this aggregate (smaller binder film thickness) along with smaller percentage of quartz (5.50%);
- It was not found much difference in the shape properties of the aggregates by means of the AIMS. For the SEM imagens, BA aggregate has a rougher texture, which might lead to better binder-aggregate physical adhesion. The influence of aggregate morphology and mineralogy on the stiffness recovery characteristics was not prominently evident. Although different minerals were observed for each aggregate, the gain in fatigue life after a rest period was the same for all studied mixtures. The authors suggested that the mineralogical effects might

become more apparent when considering moisture damage and/or more severe damage due to cracks before applying the rest period to induce more healing effects.

In conclusion, this study sheds light on the importance of fine aggregate properties in fatigue life and self-healing. The fatigue cracking and healing capacity are mainly investigated from the asphalt binder point of view, but aggregate characteristics (such as absorption, mineral type, chemical composition, and others) may impact these phenomena as well. For future studies, it suggests evaluating different rest periods as well as other factors which could affect fatigue/healing such as moisture damage and aging.

ACKNOWLEDGEMENTS

The authors would like to thank the Brazilian research agencies FAPES (Fundação de Amparo à Pesquisa e Inovação do Espírito Santo), CAPES (Coordination for the Improvement of Higher Education Personnel – Finance Code 001), and CNPq (the National Council for Scientific and Technological Development – Research Productivity Fellowship) for their financial supports to complete this study, as well as the Roads Laboratory of the São Carlos School of Engineering, University of São Paulo (USP), where part of the experimental tests were done.

REFERENCES

ABNT (2017) *NBR 16605: Cimento portland e outros materiais em pó - Determinação da massa específica.* Rio de Janeiro: ABNT.

Abo-Qudais, S. and A. Suleiman (2005) Monitoring fatigue damage and crack healing by ultrasound wave velocity, *Nondestructive Testing and Evaluation*, v. 20, n. 2, p. 125-45. DOI: 10.1080/10589750500206774.

Ayar, P.; F. Moreno-Navarro and M.C. Rubio-Gámez (2016) The healing capability of asphalt pavements: a state of the art review, *Journal of Cleaner Production*, v. 113, p. 28-40. DOI: 10.1016/j.jclepro.2015.12.034.

Babadopulos, L.F.; G. Orozco; C. Sauzéat *et al*. (2019) Reversible phenomena and fatigue damage during cyclic loading and rest periods on bitumen, *International Journal of Fatigue*, v. 124, p. 303-14. DOI: 10.1016/j.ijfatigue.2019.03.008.

Cala, A.; S. Caro; M. Lleras *et al*. (2019) Impact of the chemical composition of aggregates on the adhesion quality and durability of asphalt aggregate systems, *Construction & Building Materials*, v. 216, p. 661-72. DOI: 10.1016/j.conbuildmat.2019.05.030.

Castelo Branco, V.T.F.; E. Masad; A. Bhasin *et al*. (2008) Fatigue analysis of asphalt mixtures independent of mode of loading, *Transportation Research Record: Journal of the Transportation Research Board*, v. 2057, n. 1, p. 149-56. DOI: 10.3141/2057-18.

COD (2021) Available at: <https://www.crystallography.net/cod/> (accessed 03/09/2024).

Daniel, J.S. and Y.R. Kim (2002) Development of a simplified fatigue test and analysis procedure using a viscoelastic, continuum damage model (with discussion), *Electronic Journal of the Association of Asphalt Paving Technologists*, v. 71, p. 619-50.

Daniel, J.S. and Y.R. Kim (2001) Laboratory evaluation of fatigue damage and healing of asphalt mixtures, *Journal of Materials in Civil Engineering*, v. 13, n. 6, p. 434-40. DOI: 10.1061/(ASCE)0899-1561(2001)13:6(434).

DNIT (2006) *DNIT 031/06 - ES: Pavimentos flexíveis - Concreto asfáltico - Especificação de serviço.* Rio de Janeiro: DNIT.

DNIT (2019) *DNIT 411/2019 - ME: Pavimentação asfáltica - Misturas asfálticas - Massa específica, densidade relativa e absorção de agregado miúdo para misturas asfálticas.* Rio de Janeiro: DNIT.

Fonseca, J.F.; J.E. Sudo Lutif Teixeira; V.T.F. Castelo Branco *et al*. (2019) Evaluation of effects of filler by-products on fine aggregate matrix viscoelasticity and fatigue-fracture characteristics, *Journal of Materials in Civil Engineering*, v. 31, n. 10, p. 04019240. DOI: 10.1061/(ASCE)MT.1943-5533.0002891.

Freire, R.A.; V.T.F. Castelo Branco and K. Vasconcelos (2014) Avaliação da resistência ao trincamento de misturas asfálticas compostas por agregados miúdos com diferentes tamanhos máximos nominais, *Revista Transportes*, v. 22, n. 3, p. 117-27. DOI: 10.14295/transportes.v22i3.791.

Freire, R.A.; L.F. Babadopulos; V.T.F. Castelo Branco *et al*. (2017) Aggregate maximum nominal sizes' influence on fatigue damage performance using different scales, *Journal of Materials in Civil Engineering*, v. 29, n. 8. DOI: 10.1061/(ASCE)MT.1943-5533.0001912.

Ibiapina, D.S.; V.T.F. Castelo Branco; L. Diogenes *et al*. (2018) Proposição de um sistema de classificação das propriedades de forma de agregados caracterizados com o uso do processamento digital de imagens a partir de materiais oriundos do Brasil, *Revista Transportes*, v. 26, n. 4, p. 116-28. DOI: 10.14295/transportes.v26i4.1510.

Karki, P.; R. Li and A. Bhasin (2015) Quantifying overall damage and healing behavior of asphalt materials using continuum damage approach, *The International Journal of Pavement Engineering*, v. 16, n. 4, p. 350-62. DOI: 10.1080/10298436.2014.942993.

Kim, Y.R.; D. Little and R.L. Lytton (2003) Fatigue and healing characterization of asphalt mixtures, *Journal of Materials in Civil Engineering*, v. 15, n. 1, p. 75-83. DOI: 10.1061/(ASCE)0899-1561(2003)15:1(75).

Kim, Y.R.; D. Little and I. Song (2003) Effect of mineral fillers on fatigue resistance and fundamental material characteristics: mechanistic evaluation, *Transportation Research Record: Journal of the Transportation Research Board*, v. 1832, n. 1, p. 1-8. DOI: 10.3141/1832-01.

Klug, A.B.; A. Ng and L.A. Faxina (2022) Application of the viscoelastic continuum damage theory to study the fatigue performance of asphalt mixtures: a literature review, *Sustainability*, v. 14, n. 9, p. 4973. DOI: 10.3390/su14094973.

Li, M.; G. Wu; E. Fini *et al*. (2020) Investigating the healing capacity of asphalt mixtures containing iron slag, *Construction & Building Materials*, v. 261, p. 119446. DOI: 10.1016/j.conbuildmat.2020.119446.

Li, R.; P. Karki and P. Hao (2020) Fatigue and self-healing characterization of asphalt composites containing rock asphalts, *Construction & Building Materials*, v. 230, p. 116835. DOI: 10.1016/j.conbuildmat.2019.116835.

Li, M.; G. Wu; M. Rajib *et al*. (2023) Investigating the effect of ultraviolet aging on the healing capacity of bitumen containing taconite tailings, *Road Materials and Pavement Design*, v. 24, n. 1, p. 267-78. DOI: 10.1080/14680629.2021.2012237.

Masad, E.; L. Tashman; D. Little *et al*. (2005) Viscoplastic modeling of asphalt mixes with the effects of anisotropy, damage and aggregate characteristics, *Mechanics of Materials*, v. 37, n. 12, p. 1242-56. DOI: 10.1016/j.mechmat.2005.06.003.

Mazzoni, G.; A. Stimilli and F. Canestrari (2016) Self-healing capability and thixotropy of bituminous mastics. *International Journal of Fatigue*, v. 92, p. 8-17. DOI: 10.1016/j.ijfatigue.2016.06.028.

Moreno, F. and M.C. Rubio (2013) Effect of aggregate nature on the fatigue-cracking behavior of asphalt mixes, *Materials & Design*, v. 47, p. 61-7. DOI: 10.1016/j.matdes.2012.12.048.

Moura, B.L.R.; J.E.S.L. Teixeira; R. Simão *et al*. (2020) Adhesion between steel slag aggregates and bituminous binder based on surface characteristics and mixture moisture resistance, *Construction & Building Materials*, v. 264, p. 120685. DOI: 10.1016/j.conbuildmat.2020.120685.

Ng, A.K.Y.; A.C. Vale; A.C. Gigante *et al*. (2018) Determination of the binder content of fine aggregate matrices prepared with modified binders, *Journal of Materials in Civil Engineering*, v. 30, n. 4, p. 04018045. DOI: 10.1061/(ASCE)MT.1943-5533.0002160.

Oliveira, L.S.; L.F. Babadopulos and J.B. Soares (2021) Evolution of asphalt binder stiffness during fatigue loading and rest periods and its impact on fatigue life, *International Journal of Fatigue*, v. 144, p. 106041. DOI: 10.1016/j.ijfatigue.2020.106041.

Palvadi, S.; A. Bhasin and D. Little (2012) Method to quantify healing in asphalt composites by continuum damage approach, *Transportation Research Record: Journal of the Transportation Research Board*, v. 2296, n. 1, p. 86-96. DOI: 10.3141/2296-09.

Phan, T.M.; D. Park and T.H. Le (2018) Crack healing performance of hot mix asphalt containing steel slag by microwaves heating, *Construction & Building Materials*, v. 180, p. 503-11. DOI: 10.1016/j.conbuildmat.2018.05.278.

Pivetta, F.C.; L.A. Nascimento and L.A.T. Brito (2020) Proposta de protocolo de ensaio para análise de regeneração em misturas asfálcas através do modelo S-VECD, *Revista Transportes*, v. 28, n. 4, p. 38-52. DOI: 10.14295/transportes.v28i4.2028.

Rodrigues, J.A.; J.E.S.L. Teixeira; Y.R. Kim *et al*. (2019) Crack modeling of bituminous materials using extrinsic nonlinear viscoelastic cohesive zone (NVCZ) model, *Construction & Building Materials*, v. 204, p. 520-9. DOI: 10.1016/j.conbuildmat.2019.01.215.

Sánchez, D.B.; J. Grenfell; G. Airey *et al*. (2017) Evaluation of the degradation of fine asphalt-aggregate mixtures containing high reclaimed asphalt pavement contents, *Road Materials and Pavement Design*, v. 18, n. sup2, p. 91-107. DOI: 10.1080/14680629.2017.1304250.

Shen, S.; H.M. Chiu and H. Huang (2010) Characterization of fatigue and healing in asphalt binders, *Journal of Materials in Civil Engineering*, v. 22, n. 9, p. 846-52. DOI: 10.1061/(ASCE)MT.1943-5533.0000080.

Underwood, B.S.; C. Baek and Y.R. Kim (2012) Simplified viscoelastic continuum damage model as platform for asphalt concrete fatigue analysis, *Transportation Research Record: Journal of the Transportation Research Board*, v. 2296, n. 1, p. 36-45. DOI: 10.3141/2296-04.

Vasconcelos, K.L.; A. Bhasin and D. Little (2010) Influence of reduced production temperatures on the adhesive properties of aggregates and laboratory performance of fine aggregate-asphalt mixtures, *Road Materials and Pavement Design*, v. 11, n. 1, p. 47-64. DOI: 10.1080/14680629.2010.9690259.

Xu, G. and H. Wang (2016) Study of cohesion and adhesion properties of asphalt concrete with molecular dynamics simulation, *Computational Materials Science*, v. 112, p. 161-9. DOI: 10.1016/j.commatsci.2015.10.024.

Zhang, J.; A.K. Apeagyei; G.D. Airey *et al*. (2015) Influence of aggregate mineralogical composition on water resistance of aggregate–bitumen adhesion, *International Journal of Adhesion and Adhesives*, v. 62, p. 45-54. DOI: 10.1016/j.ijadhadh.2015.06.012.